

# DESIGN OF A GEOSYNCHRONOUS SAR SYSTEM FOR WATER-VAPOUR MAPS AND DEFORMATION ESTIMATION

Andrea Monti Guarnieri<sup>(1)</sup>, Luca Perletta<sup>(1)</sup>, Fabio Rocca<sup>(1)</sup>, Diego Scapin<sup>(1)</sup>, Stefano Tebaldini<sup>(1)</sup>, Antoni Broquetas<sup>(2)</sup>, Josep Ruiz<sup>(2)</sup>

<sup>(1)</sup> Dipartimento di Elettronica e Informazione, Politecnico di Milano. Email [monti@elet.polimi.it](mailto:monti@elet.polimi.it)

<sup>(2)</sup> Dep. of Signal Theory and Communications, Universitat Politècnica de Catalunya

## ABSTRACT

In this paper, we propose a geosynchronous SAR concept that makes use of dual frequencies to achieve WIDE and SPOT coverage, aiming at continuous monitoring of deformation and generation of water vapour maps at high space-temporal resolution.

## 1. Introduction

Geosynchronous SARs (GeoSAR) takes advantage of the slight orbit ellipticity to provide a synthetic aperture, capable of imaging twice daily the earth surface by a peculiar near south-north line of sight [1][2][3].

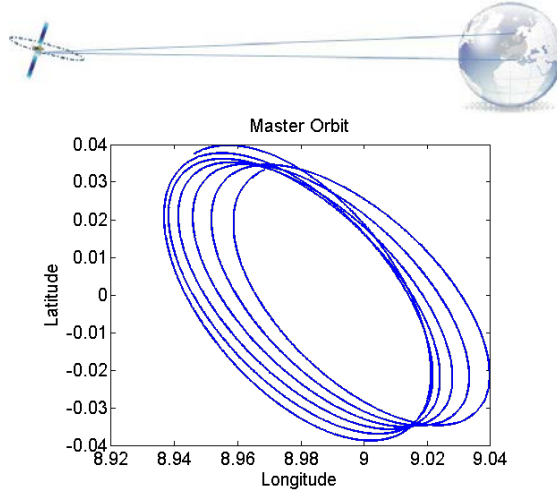


Fig. 1. Representation of a geosynchronous orbit (above) and a few days of orbits for a typical satellite (Hotbird 7), below.

The concept dates back to the 70<sup>th</sup> [1], whereby the long integration time of several hours was proposed to recover for energy backscattered from the 37000 km distance. At those time, the feasibility of such system was questionable due to the lack of information on target stability and the destructive impact of water-vapour fluctuations on the propagation. These two major stopper are now cleared out, as the long term stability of scene is assessed by three decades of earth observation from the space, and efficient techniques to compensate for the Atmospheric Phase Screen (APS) are well assessed [5][6]. Indeed one of the major objectives of such system, besides monitoring

deformations, is the estimation of water-vapour maps with high spatial and temporal resolution.

The typical orbit with respect to an earth fixed reference, shown in Fig. 1, is an ellipsis whose latitude spans, in one day, the interval:

$$\Delta_\Lambda = 2e \sin(\Omega(t - t_0))$$

where "e" is the ellipticity and  $\Omega$  the angular frequency of Earth revolution. The synthetic aperture that would result, leads to a resolution:

$$\rho_a = \frac{2R_g e}{\lambda} r$$

$R_g$  being the geosynchronous radius (42000 lm),  $\lambda$ , the wavelength and  $r$  the 1-way range. Thus, if we assume an eccentricity  $e=8\times 10^{-4}$ , that is in the range of current satellites, we could get up to 2.5 m azimuth resolution say at Ku band in the 12 hours integration time. However we could take advantage of a shorter integration time, getting **quick-looks say with 100 m resolution every 15 minutes**. The range resolution would be based on the bandwidth and independent on the time.

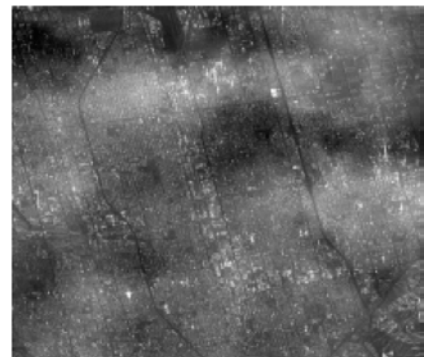


Fig. 2. Typical Atmospheric Phase Screen superposed to amplitude image, that GeoSAR could generate each 10-20 minutes.

## 2. Applications

Such a Synthetic Aperture Radar with a typical swath of hundreds to thousands of km, quick-look imaging at rates of tens of minutes and high resolution coherent imaging twice daily would open new perspectives for

applications so far unavailable but limited on-ground or airborne systems.

GeoSAR complements the spaceborne SAR systems, operated in Low Earth Orbit (LEO), in coverage: regional versus global, in revisit time hourly versus weekly, in line of sight: south-north versus east-west.

## 2.1. Water-vapour maps

GeoSAR would be able to provide water vapour maps, like the one in *Fig. 2*, useful for GPS tropospheric error removal, as well as for enhancing interferometric applications of LEO-SAR. The spatial distribution and the temporal evolution of the water vapour in the atmosphere could be captured and integrated into Numerical Weather Prediction (NWP) models. The most recent NWP models are compatible with cloud resolving modelling on spatial scales in the order of hundreds of meters, but no large scale observation technique is available that can produce high resolution initial conditions. InSAR measurements at an adequate temporal and spatial resolution could then bring significant improvement as for weather and quantitative precipitation forecasts ranging from now-casting time scales (0-6 hours) to climate change scenarios, and provide new insights about extreme meteorological events [4].

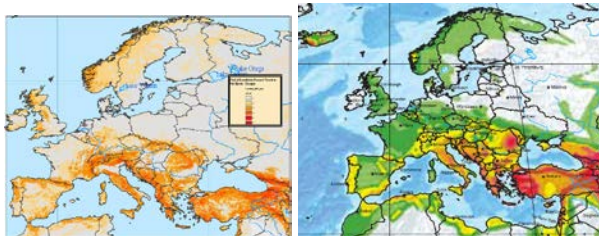


*Fig. 3. Left: number of landslides, (source: NGI), right: geoseismic risk map (source GSHAP Global Map).*

## 2.2. Deformation maps

Focusing of deformations, the primary application is the monitoring of hydro-geological and geophysical phenomena such as *landslides, seismic events, volcanic activity, and glacier dynamics*. High frequency monitoring is required in order to map rapidly changing events occurring during a volcanic eruption. Such events are generally observed through ground-based measurement systems which, however, can suffer from unfavourable looking angles and require dedicated deployment campaigns. The need for continuous acquisitions is even more urgent in areas of seismic and landslide risk, due to the unpredictability of such events. Spatial resolution is required to range from hundreds of meters, in the case of phenomena to be investigated at sub-continental scale, down to tens of meters, for the identification of smaller scale events in selected areas. Frequent InSAR measurements at proper resolution would allow matching the features of

both slow continuous and rapid intermittent movements, improving the understanding of volcanic, earthquake, and landslide processes.

Finally, as for cryospheric researches, there are still significant open issues and challenges limiting the understanding, modelling and forecasting of cryospheric processes and mass balances. The cited complementary Line of Sight orientation with respect to LEO SARs, and the choice of the Ku band would allow for the retrieval of the 3D deformation field integrating the measures of the ESA proposed explorer CoreH2O mission [5].

Last, but not least, monitoring urban deformations would take a benefit of the frequent revisit and the exploitation of users parabola as targets of opportunities, as nearly all the buildings have one them stable fixed and pointed to the geosynchronous orbit.

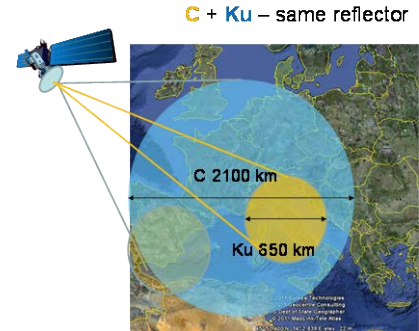


*Fig. 4. Example of coverage achievable by the WIDE and SPOT beams, by exploiting different wavelength and the same reflector.*

## 3. System design

The applications so far envisaged leads to a scenario where two different sets of requirements could be fulfilled by a Dual-Beam-Dual-Frequency system.

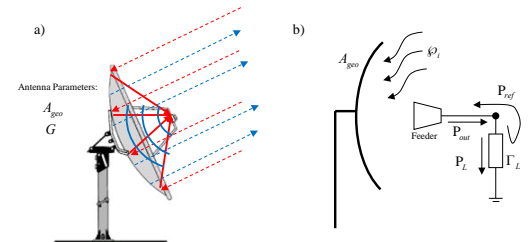


*Fig. 5. Evaluation of the RCS of home-parabola, used as reflector of opportunit: (a). (b) Feeder mismatch: power reflected and not delivered to the load.*

As for water-vapour maps, coherence is to be maximized everywhere, as well as coverage, whereas coarse resolution is acceptable. The one day revisit of ERS-Tandem mission has proven the potentials of C band for wide area coherence, with the exception of forested areas. An example is shown in *Fig. 6*. An added benefit of the long wavelength would be to

reduce the impact of atmospheric decorrelation in the long integration time [7].

On the other hand, high resolution both in azimuth and in deformations would be achieved on coherent targets, like urban and periurban areas, or non-vegetated areas, like often happens for landslides and volcanoes, by exploiting short wavelengths like Ku-band. As Ku is the one allocated for Ground Based RADAR and similar devices by ITU, there are several devices and many examples of InSAR applications in this field, proving the millimetric accuracy achievable by SARs. In Ku band, a user parabola would be highly reflective: the RCS evaluated basing on the model of Fig. 5:

$$\sigma_{ant} = \frac{4\pi}{\lambda^2} A_{geo}^2 \eta_{eff}^2 |\Gamma_L|^2$$

Thus we would achieve 23.4 dBsm at Ku-band, with a 60 m reflector (while many of them really have 80 cm diameters), by assuming  $\eta_{eff}=0.7$  and  $\Gamma_L=-10$  dB.

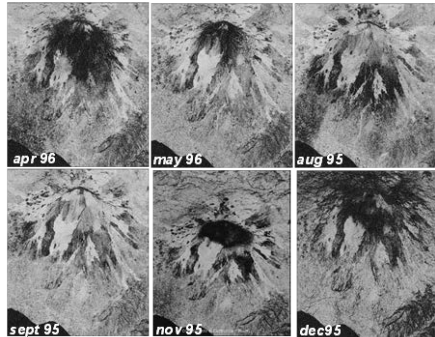


Fig. 6. Upper image: coherence maps in one-day revisit C band, from ERS-Tandem mission [6]. Lower image is night lights in Europe (NASA/GSFC) giving an idea of coherence in high frequency like Ku-band.

The synergy of the DBDF approach would be relevant in the compensation of the APS, estimated from C band WIDE swath and applied to the Ku band SPOT swath, and in the unwrapping of the deformation fringes. The WIDE and SPOT beams are represented in Fig. 4: notice that for a geosynchronous system it could be possible to design the antenna so that beams can be repositioned according to the need.

The major parameters involved in the design are summarized in Tab. I.

TABLE I  
GEOSAR PARAMETERS

	SPOT	WIDE
<b>Center swath</b>	Roma	Milano
<b>Ground swath width</b>	km	650 2100
<b>Azimuth Resolution</b>	m	10 20
<b>Ground Range Resolution</b>	m	5 20
<b>Frequency</b>	GHz	17.2 5.3
<b>Orbit accuracy</b>	deg	0.21
<b>Slant range</b>	km	37659 37954
<b>Incidence angle</b>	deg	48.49 52.32
<b>Antenna diameter</b>	m	1.53
<b>Duty cycle</b>	%	10 10
<b>PRF</b>	Hz	7-250 7-70
<b>Bitrate</b>	Mbits/s	8 2
<b>Peak power</b>	dBW	36.0 36.0
<b>W</b>		4000 4000
<b>Tx antenna directivity</b>	dB	48.8 39.4
<b>Path loss 2-way</b>	dB	-325.0 -325.2
<b>Area in antenna beam or pulse</b>	dB	108.8 118.9
<b>Atmo losses 2-way</b>	dB	-0.4 0.5
<b>Rx Eq. Antenna area</b>	dB	0.6 1.5
<b>Rx power</b>	dBW	-144.3 -143.2
<b>SNR at receiver</b>	dB	-18.4 -11.0
<b>Mean sigma_0</b>	dB	-11.1 -12.4
<b>RES/SNR FOCUSED</b>	dB	14.7 24.5
<b>SNR (9 hours)</b>	dB	2.3 1.5
<b>NESZ</b>	dB	-13.4 -13.9
<b>SNR (10 min)</b>	dB	5.7 1.1
<b>Sensitivity User Parabola</b>		
<b>Diameter</b>	cm	80
<b>Losses feeder</b>	dB	-10.0
<b>RCS</b>	dB	25.8
<b>SNR peak (12 hours)</b>		22.2
<b>SNR peak 10'</b>		4.8

The on-board electronics can be made rather simple by 1-bit quantization [2], then just by sampling and thresholding, and by re-using the received data as the next pulse in place of a chirp.

The range and azimuth resolutions have been tuned to get near 0 dB SNR, thus better performances can be achieved at coarser resolutions

The variation of the incidence angle and the ground resolution are represented in Fig. 5 for a satellite at 9° longitude: notice that performances gently degrade up to central Europe, whereas for north Europe the incidence is too large to have a reliable measure of vertical deformations.

Notice the very low velocity, in a fixed earth frame, that peaks at less than 5 m/s, three order of magnitude lower than LEO satellite. GeoSAR antenna is designed for power and not for ambiguities, and it could be very small if enough energy is achieved: the design here proposed exploits an average power of 400 W with very good performances. GeoSAR could use wide

range of PRF, from 5 Hz to tens, with a very low ambiguity ratio.

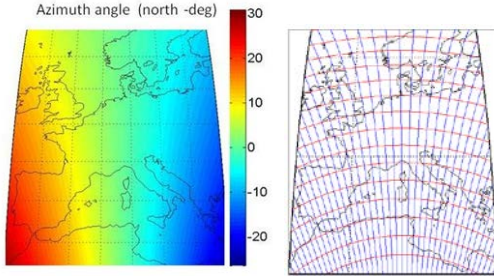


Fig. 7. Variation over Europe of the incidence angle, left, and of the ground resolution in the iso-Doppler, iso-chrones grid on the right.

#### 4. Impact and compensation of the APS

The atmospheric delay affects the phase of the raw data, that can be modelled – for a fixed range bin,  $r$ , as:

$$y(t, r) = \int_L a(\xi, r) e^{j\phi_{aps}(\xi, t)} e^{j\phi_r(\xi, t)} d\xi \quad (1)$$

$y$  being the raw data,  $t$  time along track,  $L$  the antenna footprint on the ground and  $\phi_{aps}$ ,  $\phi_r$  the two phase terms due to APS and 2-way travel time. Without loss of generality, we ignore the quadratic phase contribution of conventional SAR in straight orbit, as we are interested in short time intervals. Thus the travel path delay is approximated linear with azimuth location of the target,  $\zeta$ :

$$\begin{aligned} \phi_r(\xi, t) &= \phi_0 + 2\pi f \xi \\ f &= \frac{4\pi}{\lambda} \frac{v_s}{r_0} t = kt \end{aligned} \quad (2)$$

In absence of the phase screen, the raw data is just the Fourier transform of the source reflectivity, like for Ground Based Radar [8], where focusing by matched filter is just an inverse Fourier Transform in azimuth

$$y(t, r) = \mathbf{f}\{a(x, r)\}_{t=\frac{f_a}{k}} \Rightarrow a(x, r) = \mathbf{f}^{-1}\{y(t, r)\}$$

In LEO SAR, the acquisition time  $t_0$  lasts for less than a second, hence the phase screen is constant and modifies the source reflectivity in (1):

$$y(t, r) = \mathbf{f}\{a(x, r)e^{j\phi_{aps}(x, t_0)}\}_{t=\frac{f_a}{k}}$$

Focusing is correctly accomplished, but leaving a phase screen frozen at the acquisition time. In the GeoSAR case, the two phase fields in (1) combine so that it would not be possible to focus, unless both are known. Furthermore the retrieval of the 2D time, azimuth atmospheric phase field from the 1D raw data at a fixed range bin is, in the general case, an ill conditioned problem, even if we assume knowledge of the Doppler phase  $\phi_r$  and the backscatter  $a(x, r)$ . Nonetheless, the phase screen can be estimated and compensated by assuming that it is a very smooth function of time, and then by sub-aperture processing

[9]. Subapertures time support should be short as to provide a quick-look in which the atmosphere is frozen, thus it could be estimated as for LEO SAR, and eventually removed.

If we compensate the travel path in a subaperture of time extent  $T$ , we have from (1):

$$u(x) = \int_T y(\tau) e^{-j2\pi k \tau} d\tau = \int_T \int_L a(\xi) e^{j\phi_{aps}(\xi, \tau)} e^{j2\pi k(\xi-x)\tau} d\xi d\tau$$

We can then evaluate the impact on the focused signal amplitude by taking expectation:

$$\begin{aligned} E[u(x)u^*(x)] &= \int_L \int_T \int_T E[a(\xi_1)a^*(\xi_2)] E[e^{j[\phi_{aps}(\xi_1, \tau_1) - \phi_{aps}(\xi_2, \tau_2)]}] \\ &\quad e^{j2\pi k(\tau_1\xi_1 - \tau_2\xi_2)} d\xi_1 d\xi_2 d\tau_1 d\tau_2 \end{aligned}$$

Eventually, we assume an homogeneous distributed target that is independent and unitary amplitude:

$$\begin{aligned} \sigma_u^2(x) &= \int_T \int_L \int_E E[e^{j(\phi_{aps}(\xi, t+\Delta_t) - \phi_{aps}(\xi, \Delta_t))}] e^{j2\pi k \tau \xi} e^{-j2\pi k \xi \Delta_t} d\tau d\Delta_t d\xi \\ &= \int_T \int_L \int_E E[e^{j(\Delta \phi_{aps}(\Delta_t))}] e^{j2\pi k \tau \xi} e^{-j2\pi k \xi \Delta_t} d\tau d\Delta_t d\xi \end{aligned}$$

where  $\Delta t = \tau_2 - \tau_1$  and  $\Delta t = t_2 - t_1$ . As the differential APS is assumed normal distributed [5]:

$$\begin{aligned} \Delta \phi_{aps}(t, x) &\sim N(0, \sigma_{aps}^2(t, x)) \\ \sigma_{aps}^2(t, x) &= \left(\frac{4\pi}{\lambda}\right)^2 \left( \sqrt{\left(\frac{t}{t_0}\right)^2 + \left(\frac{|x|}{x_0}\right)^2} \right) \end{aligned} \quad (4)$$

$t_0$  being dependent on the atmospheric turbulence, we get:

$$\sigma_u^2(x) = \int_T \int_L \int_E e^{\frac{\sigma_{aps}^2(t)}{2}} e^{j2\pi k \tau \xi} e^{-j2\pi k \xi \Delta_t} d\tau d\Delta_t d\xi \quad (5)$$

When we are in absence of atmospheric phase field, we have the usual SAR impulse response function:

$$\begin{aligned} \sigma_u^2(x) &= \int_{T+\tau} \int_L \int_E e^{-j2\pi k \xi \Delta_t} d\xi d\Delta_t \int_T e^{j2\pi k \xi \tau} d\tau \\ &= \sigma_a^2 \int_L \text{sinc}(kT\xi) d\xi \int_T e^{-j2\pi k \xi \Delta_t} d\Delta_t = \text{sinc}^2(kTx) \end{aligned}$$

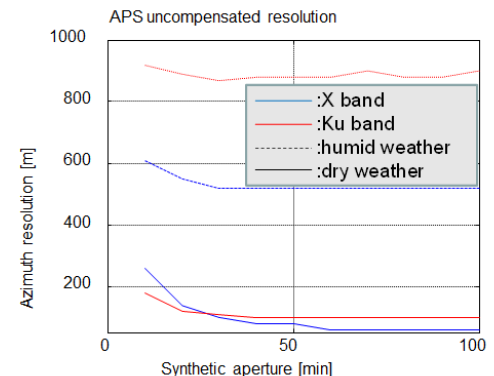


Fig. 8. Resolution achieved as function of the subaperture by accounting for the atmospheric phase field by assuming a typical winter (above) and summer (below) weather.

Whereas in general we experience a resolution loss. The achievable resolution by (5) has been plotted in Fig. 8 by exploiting the APS variogram averaged in winter ( $300 \text{ mm}^2$  in one day, thus) and summer ( $1000 \text{ mm}^2$ ) in humid area of Como. Notice that resolution worsen by increasing the frequency. However, it is sufficient to exploit X band, to get a resolution better than the APS lobe even in the worst case. Thus X-band could provide an alternative to the 2 band approach here proposed.

The actual size of the temporal window should be optimized as a compromise between the spatial decorrelation, due to the atmospheric turbulence in the azimuth resolution, and the temporal decorrelation in the sub-aperture time. Therefore, the total coherence is:

$$\gamma = \gamma_s \times \gamma_t = \exp\left(-\frac{1}{2}\left(\frac{4\pi}{\lambda}\right)^2 \frac{T}{t_0}\right) \exp\left(-\frac{1}{2}\left(\frac{4\pi}{\lambda}\right)^2 \frac{X}{x_0}\right) \quad (6)$$

and by exploiting the relation between the subaperture and the focused extents:

$$T \times X = \frac{\lambda R}{2v}$$

that can be plugged in (6) giving the optimal subaperture:

$$T = \sqrt{\frac{\lambda R}{2v} \frac{t_0}{x_0}}$$

that is 14 minutes in X band or 21 in C band. These values are compatible with the present design in Tab. I.

## 5. Conclusions

A geosynchronous SAR system has been presented. The design makes use of two different frequencies illuminating the same reflector, thus achieving simultaneous observations over a WIDE are and a SPOT one. The WIDE beam is suited to estimate water-vapour maps, that can be used for numerical weather forecast and for compensation of the atmospheric phase screen in other LEO-SAR and GPS. The coarse resolution phase field estimate in WIDE beam is exploited in the SPOT beam to remove the APS and to solve for wrapping of fringes from fast displacements. The fine resolution achieved in that beam by the use of Ku band, together with the high sensitivity to displacement makes the system quite suited for continuous monitoring of hazardous areas, exposed to seismic activity and landslides.

## References

- [1] K. Tomiyasu, *Synthetic aperture radar in geosynchronous orbit*. IEEE Antennas and Propagation Symp., U.Maryland, pp.42-45, May 1978.
- [2] Claudio Prati, Fabio Rocca, Diego Giancola, and Andrea Monti Guarnieri. Passive geosynchronous SAR

system reusing backscattered digital audio broadcasting signals. *IEEE Transactions on Geoscience and Remote Sensing*, 36(6):1973-1976, 1998.

[3] N Madsen, Wendy Edelstein, Leo D Di Dominico, and John LaBrecque. A geosynchronous synthetic aperture radar; for tectnoci mapping, disaster management and measurements of vegetation and soil moisture. In *International Geoscience and Remote Sensing Symposium*, Sydney, Australia, 9-13 July 2001.

[4] Ferretti, A., Prati, C., Rocca, F. (2001). *Permanent Scatterers in SAR Interferometry*. *IEEE Trans. Geoscience And Remote Sensing*, 39(1), 8 - 20.

[5] Ramon F. Hanssen. *Radar Interferometry: Data Interpretation and Error Analysis*. Springer Verlag, Heidelberg, 2 edition, 2005.

[6] Nazzareno Pierdicca et. Al, *Numerical weather prediction models and SAR interferometry: synergic use for meteorological and INSAR applications* Antennas and Propagation (EUCAP), Proceedings of the 5th European Conference on , vol., no., pp.3247-3250, 11-15 April 2011.

[7] ESA, *CoReH2O Earth Explorer Core Mission*, Mission Requirements Document, EOP-SM/2007/MK, May 2009

[8] A Ferretti, C Prati, F Rocca, and A Monti Guarnieri. *Multibaseline SAR interferometry for automatic DEM reconstruction*. In *Third ERS Symposium-Space at the Service of our Environment*, Florence, Italy, 17-21 March 1997, ESA SP-414, pages 1809-1820, 1997..

[9] Guarnieri, A.M.; Rocca, F.; Ibars, A.B.; , *Impact of atmospheric water vapour on the design of a Ku band geosynchronous SAR system*, *Geoscience and Remote Sensing Symposium,2009, IGARSS 2009* , vol.2, no., pp.II-945-II-948, 12-17 July 2009

[10] Guarnieri, A.M and S. Scirpoli. *Efficient wavenumber domain focusing for ground-based SAR*. *Geoscience and Remote Sensing Letters*, IEEE, 7(1):161 -165

[11] S. Tebaldini, A. Monti Guarnieri, F. Rocca *Recovery of Time and Space Varying Phase Screens in SAR*, EUSAR 2012.